MAGNETIC RESONANCE IN CHEMISTRY
Magn. Reson. Chem. 2005; **43**: S119–S129
Published online in Wiley InterScience (www.interscience.wiley.com). DOI: 10.1002/mrc.1677

Molecular dynamics of nitroxides in glasses as studied by multi-frequency EPR†

Evgeniya P. Kirilina,[1,3] Thomas F. Prisner,[2] Marina Bennati,[2] Burkhard Endeward,[2] Sergei A. Dzuba,[1] Martin R. Fuchs,[3] Klaus Möbius[3] and Alexander Schnegg[3,4]*

[1] Institute of Chemical Kinetics and Combustion, Institutskaya 3, Novosibirsk, 630090, Russia
[2] Institut für Physikalische und Theoretische Chemie, Johann Wolfgang Goethe Universität, Marie Curie Strasse 11, 60439 Frankfurt, Germany
[3] Freie Universität Berlin, Arnimallee 14, 14195 Berlin, Germany
[4] Max-Planck Institut für Bioanorganische Chemie, Stiftstrasse 34-36, 45470 Mülheim an der Ruhr, Germany

Received 25 April 2005; Revised 14 June 2005; Accepted 16 June 2005

Pulsed multi-frequency EPR was used to investigate orientational molecular motion of the nitroxide spin probe (Fremy's salt) in glycerol glass near the glass transition temperature. By measuring echo-detected EPR spectra at different pulse separation times at resonance frequencies of 3, 9.5, 95 and 180 GHz, we were able to discriminate between different relaxation mechanisms and characterize the timescale of molecular reorientations (10^{-7}–10^{-10} s). We found that near the glass transition temperature, the orientation-dependent transverse relaxation is dominated by fast reorientational fluctuations, which may be overlapped with fast modulations of the canonical g-matrix values.

The data was interpreted using a new simulation program for the orientation-dependent transverse relaxation rate $1/T_2$ of nitroxides based on different models for the molecular motion. The validity of the different models was assessed by comparing least-square fits of the simulated relaxation behaviour to the experimental data.

KEYWORDS: pulsed multi-frequency EPR; Fremy's salt; nitroxide; high-field/high-frequency EPR; glass transition; orientational molecular motion

INTRODUCTION

The molecular motion properties of supercooled liquids or glasses, which determine their amorphous rigidity around the glass transition temperature T_g, are still not fully understood.[1,2] The ordering process in glassy media in this temperature range is accompanied by characteristic motional modes that are due to a hopping process between the minima of a multidimensional potential energy surface.[2] The interest in the dynamics of supercooled liquids strongly increased when it was shown that fluctuations in glasses can be successfully used as a model for describing the dynamics of proteins with their complicated energy landscapes.[3] A thorough understanding of these energy landscapes is indispensable for modeling both protein folding[3] and protein function.[4,5] As a fundamental characteristic, glasses show a qualitative change in the underlying dynamics at T_g. Upon approaching this limit, the glass molecules are trapped in rigid sub-units called *cages*. These cages perform a collective large-scale motion, which determines the flexibility of the glass. In the cage, the molecular motion is hindered by structural constraints that allow only restricted small-angle fluctuations around the equilibrium position of the molecule, usually referred to as *librations*. An important tool to gain detailed information about molecular dynamics in glasses is electron paramagnetic relaxation studies.[6–17]

In the work presented, we used echo-detected electron paramagnetic resonance (ED-EPR) at different resonance frequencies to study the influence of molecular motion on the transverse relaxation time of a nitroxide spin probe, the peroxylamine disulphonate ion $[(SO_3)_2NO]^{2-}$ of the well-known Fremy's salt,[18] in frozen glycerol glass. The relaxation of the electron magnetization is coupled to the orientational motion of the spin probe via motion-induced fluctuations of the effective hyperfine and *g*-values. These fluctuations can be induced by reorientations of the magnetic interaction tensors or by modulation of the elements of the tensor matrices. Thus, molecular motion leads to stochastic Larmor frequency fluctuations, which can be characterized by a motional correlation time τ_c and an amplitude $\Delta\omega$ that depends on the orientation of the radical relative to the external magnetic field $\boldsymbol{H}_o$. In the present article, relaxation that depends on the resonance position in the ED-EPR spectrum is called *anisotropic*, whereas relaxation that is uniform over the whole spectrum is called *isotropic*. By measuring the

†**Presented as part of a special issue on High-field EPR in Biology, Chemistry and Physics.**

*Correspondence to: Alexander Schnegg, Freie Universität Berlin, Arnimallee 14, 14195 Berlin, Germany.
E-mail: alexander.schnegg@physik.fu-berlin.de

Contract/grant sponsor: INTAS; Contract/grant number: YSF 2002-410/F1b.
Contract/grant sponsor: Deutsche Forschungsgemeinschaft; Contract/grant number: SPP 1051, SFB 498.
Contract/grant sponsor: Russian Foundation for Basic Research; Contract/grant number: 04-03-32211.

transverse relaxation rates at different resonance positions and thereby selecting different orientations of the spin probe, these processes can be characterized and, moreover, discriminated from orientation-independent relaxation mechanisms such as methyl group rotation[14,19] and nuclear spin dynamics.[12,14,20] In frozen solution, orientation-dependent relaxation may be induced by the collective motion of the solvent cage,[13] reorientational molecular motion within the cage[21] or dynamic *A*- and *g*-strains.[22] In recent ED-EPR studies, it was shown that far below the glass transition temperature T_g, fast restricted motion ($\sim 10^{-9}$ s) dominates the anisotropic relaxation.[11,12,21,23–25] At temperatures above T_g, the relaxation is more and more induced by slow ($\sim 10^{-6}$ s) molecular orientational diffusion.[8,13,17,26]

Nevertheless, ambiguities in the interpretation of ED-EPR data remained for temperatures close to the glass transition where the regimes of slow unrestricted motion and fast restricted motion may overlap. To obtain further insight into the character of the motional process that dominates the transverse relaxation at this temperature, we performed measurements of the transverse relaxation rates at different resonant frequencies ω_o (S(3 GHz)-, X(9.5 GHz)-, W(95 GHz)- and G(180 GHz)-bands). This multi-frequency approach is analogous to modern NMR where multi-frequency measurements of the relaxation times help draw a detailed picture of molecular motions.[27] The accessible time window for NMR, however, is generally much slower than that for EPR. Pulsed multi-frequency EPR measurements at different Zeeman frequencies, which are necessary to extract the full information content, have become possible only recently, through the development of new pulsed high-field EPR spectrometers.[28–31]

The timescale of the relaxation-inducing motional process

The first step for extracting information about the motional process from measurements of the transverse relaxation rates is to determine the timescale of the motion.

For relaxation induced by stochastic processes, the phase memory time T_2 is a non-monotonous function of the correlation time of the fluctuations. It reaches its minimum at $\Delta\omega\tau_c \approx 1$. This limit separates the timescales of motion into the fast-motion, i.e. motional narrowing regime ($\Delta\omega\tau_c \gg 1$) and the slow-motion regime ($\Delta\omega\tau_c \ll 1$). In both regimes, the time constant of the echo decay depends monotonously on the correlation time of the stochastic process. However, an assignment of the measured relaxation time to one of the two regimes is complicated by the fact that the transverse relaxation rate $1/T_2$ is a function of both $\Delta\omega$ and τ_c, which cannot be extracted independently from pulsed EPR measurements at only one microwave frequency.

Additional information about the motional process can be obtained by measuring the relaxation rate at different resonance frequencies. For relaxation induced by changes of the effective *g*-value, the amplitude of the Larmor frequency fluctuations increases by increasing the external magnetic field. In the following, we will discuss how the field dependence of the relaxation process can be used to extract information about the timescale of the motion.

Fast molecular motion leads to mono-exponential echo decays that can be characterized by the transverse relaxation rate $1/T_2$. The dependence of $1/T_2$ on the amplitude of the Larmor frequency fluctuations $\Delta\omega$ and the correlation time τ_c follows the simple expression:[32]

$$\frac{1}{T_2} = \overline{\Delta\omega^2}\tau_c \qquad (1)$$

where the bar indicates time averaging.

In the slow-motion regime, different types of molecular motion lead to different echo-decay functions. Slow molecular motion often leads to non-exponential decay and no general expression for the dependence of the phase memory time on $\Delta\omega$ and τ_c can be derived. Nevertheless, criteria whether the observed relaxation is induced by fast or slow molecular motion can be extracted from the fact that slow motion does not lead to mono-exponential decays and a quadratic dependence of $1/T_2$ on $\Delta\omega$ at the same time. This conclusion was drawn by a comparison of the theoretical studies summarized in Table 1.

The echo-decay functions for spin 1/2 systems with anisotropic **g**-matrix that are given in Table 1 have been derived by Schwartz *et al.*[33] and Zhidomirov *et al.*[34] using different theoretical approaches. The expressions taken from Ref. 33 are based on a numerical method developed by Freed

Table 1. Theoretically derived echo-decay functions for a two-pulse $\pi/2$-τ–π-τ sequence for different types of slow molecular motion of a spin 1/2 system with anisotropic **g**-matrix. In the expressions, τ and τ_c are the pulse separation time and the motional correlation time respectively. The parameters *A*, *B* and *C*, which contain the field dependence of the echo-decay functions, are: $A = 2\gamma_e(\partial\widehat{\boldsymbol{H}}/\partial\theta)^2 D/3$, with the electron gyromagnetic ratio γ_e, the diffusion coefficient of the orientational motion *D* and the angular gradient of the Hamiltonian, $\partial\boldsymbol{H}/\partial\theta \propto H_0$; $B = 2(F/\tau_c)^{1/2}$; and $C = 2(F/\tau_c^2)^{1/3}$; respectively. $F = 2\gamma_e H_0(g_{xx} - g_{zz})/3$ quantifies the Larmor frequency fluctuations during the molecular reorientations

Motional model	Echo-decay function	References
Brownian diffusion ($\tau < 1/F$)	$\exp(-A\tau^3)$, $A \propto H_0^2$	33–35
Brownian diffusion ($\tau > 1/F$)	$\exp(-B\tau)$, $B \propto H_0^{1/2}$	33
Free diffusion	$\exp(-C\tau)$, $C \propto H_0^{1/3}$	33
Two-site jump, sudden jumps	$\exp\left(-\frac{2\tau}{\tau_c}\right)$	33, 34, 36

and co-workers[13,33,37,38] to calculate the impact of molecular motion on the EPR line shape. By solving the stochastic Liouville equation, which describes both the reversible spin dynamics and the irreversible molecular dynamics, they were able to calculate echo-decay functions for different types of fast and slow molecular motion. Following this approach, Schwartz *et al*. simulated echo-decay functions for several models of slow molecular reorientation.[33]

A different approach was applied by Zhidomirov *et al*. who derived analytical expressions for the echo decays[34] for different types of stochastic fluctuations of the secular part of the spin Hamiltonian, i.e. fluctuations of the Larmor frequency.

Molecular motion can either occur as orientational diffusion in infinitesimal steps (Brownian diffusion model) or as finite jumps between different orientations (jump models). For Brownian diffusion, a cubic dependence of the echo-decay function on τ for short pulse separation times[33,34] is predicted, whereas for longer pulse separation times, the decay function has a mono-exponential asymptote, with a decay rate proportional to $H_0^{1/2}$.[33]

These results were recently confirmed theoretically by Leoporini *et al*.[17] By deriving expressions for the echo decays at the canonical **g**-matrix positions, the authors found mono-exponential decay functions with relaxation rates showing a square-root dependence on the external magnetic field (Eqns 13–15, A1–A3 in Ref. 17).

Jump models including jumps between two discrete positions[34] and jumps between random orientations of the molecule have been developed.[33] In both cases, in the slow-motional regime, the relaxation is isotropic, and the relaxation rates are only determined by the correlation time (Table 1).

In addition, a combination of diffusion and jumps termed *free diffusion*[33] has been discussed, which results in a mono-exponential echo decay and $\boldsymbol{H}_0^{1/2}$ dependence of the decay function.

Summarizing the results from the various approaches described above, we draw the conclusion that only fast molecular motion leads to both a mono-exponential decay and a quadratic dependence of the echo-decay function on the EPR resonance frequency. It should be added that in nitroxides an additional contribution of the nitrogen hyperfine interaction has to be taken into account for an exact calculation of the transverse relaxation rates. In W-band (95 GHz) and G-band (180 GHz) EPR, however, where the line shape is dominated by the **g**-matrix anisotropy, the contribution of the hyperfine component can be neglected, and the expressions in Table 1 are good approximations. Therefore, measuring the echo-decay functions at high magnetic fields of different magnitudes provides decisive criteria for whether the observed transverse relaxation is induced by fast or slow molecular motion.

The orientation dependence of the motional process

The second important advantage of multi-frequency measurements on molecules with anisotropic **g**- and **A**-tensors arises from the option of orientation selection, allowing for the determination of the main directions of the molecular excursions. For nitroxides, the line shape of the EPR spectrum is determined by the field-dependent electron Zeeman interaction term and the field-independent hyperfine interaction with the nuclear spin of the nitrogen. In isotropic frozen solution, all orientations of the molecule contribute to the EPR spectrum. By using soft microwave pulses that excite only a defined fraction of spins in the spectrum, orientation-selective measurements of the transverse relaxation rates can be performed.[39] At sufficiently high magnetic fields, the spectral width is dominated by the anisotropic Zeeman interaction and the components of the **g**-matrix become resolved, which leads to enhanced orientation selection. At the low-field edge of the spectrum, orientations of the molecules with their *x*-axis perpendicular to the external magnetic field are selected, while at the high-field edge the *z*-orientations contribute. At the maximum of the spectrum, the *y*-orientation is predominantly selected. In our study, we compare the anisotropic relaxation at four different frequency bands, 3 GHz (S), 9.5 GHz (X), 95 GHz (W) and 180 GHz (G). By simultaneous simulation of the field-swept ED-EPR spectra obtained at four different resonance frequencies and at different pulse separation times, we were able to discriminate between motions about different molecular axes (see the section on *Results and Discussion*).

MATERIALS AND METHODS

Fremy's salt was synthesized by I. E. Sokolov (Institute of Chemical Kinetics and Combustion, Novosibirsk). The structure of Fremy's salt is shown in Scheme 1. Glycerol was purchased from Aldrich Ltd (purity 99.5%). Fremy's salt was dissolved in water, rapidly mixed with glycerol and then shock-frozen to 77 K to conserve the radicals. The water concentration was below 5%. The nitroxide concentration was below 1 mM.

The pulsed EPR measurements were performed with laboratory-built spectrometers operating in S-band,[40] W-band[28,41] and G-band.[30] For the X-band measurements, a commercial Bruker ESP-380 FT EPR spectrometer was used. The spectra were recorded with a $\pi/2$-τ–π-τ pulse sequence while stepping the external magnetic field. Each ED-EPR spectrum was recorded at different pulse separation times. The $\pi/2$ pulse lengths were 148 ns (S-band), 32 ns (X-band), 55 ns (W-band) and 100 ns (G-band), respectively. The S-band pulses were chosen this long to suppress the strong ESEEM modulations of the echo decays from hyperfine interaction with the proton nuclear spins at this low frequency.

All experiments were performed at a temperature of 185 K. To control the sample temperature at X-band and

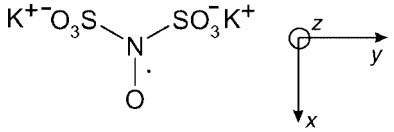

Scheme 1. Molecular structure of the nitroxide Fremy's salt and the orientation of the **g**-matrix axes with respect to the molecular frame.

W-band, the ER 4111 VT unit (Bruker) was used and at S- and G-bands, a helium cryostat (Oxford Cryosystems Ltd) was used. The sample temperature was monitored with a Cu–constantan thermocouple. The thermocouple was placed in the sample tube during the S- and X-band measurements and in the vicinity of the resonator during the W- and G-band experiments. This set-up provided temperature stability of ±1 K. The simulations were done in two steps. First, the *g*- and hyperfine values were extracted from numerical fits of the simulated spectra to the solid-state continuous-wave (cw) spectra obtained at W-band. In a second step, the motional parameters were obtained by simultaneously fitting the 2D echo-detected S-, X-, W- and G-band spectra. The fitting algorithm was based on a least-squares fitting routine from the Matlab suite (The Mathworks). Since isotropic relaxation was neglected, all spectra have been normalized to their maximum amplitude.

THEORY AND SIMULATIONS

EPR spectra of nitroxides in frozen solution

In the following subsection, we describe the theoretical expressions we used to simulate the influence of fast, restricted molecular reorientations on the ED-EPR spectrum.

The spin Hamiltonian at a nitroxide molecule can be formulated as:

$$\hat{\boldsymbol{H}} = \beta \boldsymbol{H}_0 \mathbf{g} \hat{\boldsymbol{S}} - \beta_N \boldsymbol{H}_0 \hat{\boldsymbol{I}}_N + \hat{\boldsymbol{I}} \mathbf{A} \hat{\boldsymbol{S}} \tag{2}$$

where the first term is the electron Zeeman interaction between the electron spin and the external magnetic field $\boldsymbol{H}_0$, β is the Bohr magneton, $\mathbf{g}$ is the anisotropic $\mathbf{g}$-matrix. The second term describes the nuclear Zeeman interaction of the nitrogen nuclear spin operator $\hat{\boldsymbol{I}}_N$ with the external magnetic field; β_N is the nuclear magneton of the nitrogen. The third term is the hyperfine interaction between the spins of the electron and the nitrogen, quantified by the anisotropic hyperfine tensor $\mathbf{A}$.

The energy levels of the Hamiltonian can be obtained from first-order perturbation theory taking the secular part of the electron Zeeman interaction as zero-order approximation of the Hamiltonian and the nuclear Zeeman and the hyperfine interactions as the first-order perturbations (Fig. 1):

$$E_{M_I} = \pm \frac{\beta g^*_{zz} |\boldsymbol{H}_0|}{2} + M_I \frac{|\boldsymbol{a}_\pm|}{2} \tag{3}$$

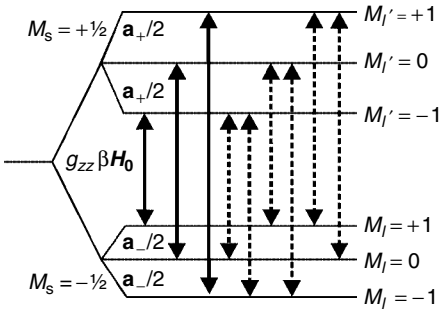

Figure 1. Energy levels of a nitroxide radical split by an external magnetic field. The arrows indicate allowed ($M_I = -M'_I$ solid) and forbidden ($M_I \neq -M'_I$ dashed) EPR transitions.

where the sign corresponds to the sign of the projection of the electron spin on the direction of the external magnetic field $\boldsymbol{H}_0$. M_I is the projection of the nuclear spin on the direction of the effective magnetic field, $\boldsymbol{a}_\pm$ is the value of the effective magnetic field at the nucleus, given by the vector sum of the external field $\boldsymbol{H}_0$ and the hyperfine field $\mathbf{A}\hat{\mathbf{S}}$. It has two different values depending on the projection of the electron spin on the direction of external magnetic field. g^*_{zz} is the *z*-component of the $\mathbf{g}$-matrix in the laboratory frame. The dependence on g^*_{zz} and $\boldsymbol{a}_\pm$ in the polar angles φ and θ, which define the orientation of the external magnetic field in the molecular frame, is given by the following expressions:

$$g^*_{zz} = g_{xx} \sin^2\theta \cos^2\varphi + g_{yy} \sin^2\theta \sin^2\varphi + g_{zz} \cos^2\theta \tag{4}$$

$$\boldsymbol{a}_\pm = \begin{bmatrix} \left(A_{xx} \cos^2\varphi + A_{yy} \sin^2\varphi - A_{zz}\right) \sin\theta \cos\theta \\ \left(A_{yy} - A_{xx}\right) \sin^2\varphi \sin\theta \\ A_{xx} \cos^2\varphi \sin^2\theta + A_{yy} \sin^2\varphi \sin^2\theta \\ + A_{zz} \cos^2\theta \pm \gamma_N \boldsymbol{H}_0 \end{bmatrix} \tag{5}$$

where g_{ii} and A_{ii} are the canonical values of the $\mathbf{g}$- and hyperfine tensors, respectively, γ_N nuclear gyromagnetic ratio, $\boldsymbol{H}_0 = |\boldsymbol{H}_0|$.

The resonant fields of the nine transitions between the levels in Eqn (3) are:

$$\begin{aligned} H_{res}(\theta, \phi, M_1, M'_1) &= \frac{1}{\beta g^*_{zz}(\theta, \phi)} \left(\hbar\omega_0 - M_1 \frac{|a_+|}{2} - M'_1 \frac{|a_-|}{2} \right) \\ &= \frac{\hbar\omega_0}{\beta g^*_{zz}(\theta, \phi)} - M_1 \frac{|a_+|}{2\beta g_e} - M'_1 \frac{|a_-|}{2\beta g_e} \end{aligned} \tag{6}$$

In Eqn (6), we used $g_e/g^*_{zz}(\theta, \varphi) = 1$ since g_{zz} is close to the free electron *g*-factor g_e.

From Eqn (6) it can be seen that at low magnetic fields, i.e. low ω_0, the spectral shape is mainly determined by the field-independent hyperfine interaction, while at higher ω_0 the equation is dominated by the $\mathbf{g}$-matrix anisotropy.

The transition probability P_{M_I, M'_I} for every orientation is determined by the angle Ω between the two possible directions of the effective magnetic fields at the nuclear spin $\boldsymbol{a}_+$ and $\boldsymbol{a}_-$:

$$\cos(\Omega(\theta, \varphi)) = \frac{\boldsymbol{a}_+ \boldsymbol{a}_-}{|\boldsymbol{a}_+||\boldsymbol{a}_-|} \tag{7a}$$

$$P_{1,-1}, P_{-1,1} = \left(\frac{1 - \cos\Omega}{2} \right)^2 \tag{7b}$$

$$P_{1,0}, P_{-1,0}, P_{0,1}, P_{0,-1} = \frac{1 - \cos^2\Omega}{2} \tag{7c}$$

$$P_{1,1}, P_{-1,-1} = \left(\frac{1 + \cos\Omega}{2} \right)^2 \tag{7d}$$

$$P_{0,0} = \cos^2\Omega \tag{7e}$$

In S- and X-bands, Ω is close to 180° and only the $M_I = M'_I$ transitions have to be taken into account when simulating the EPR spectrum, while at higher resonance frequencies, additionally the $M_I \neq -M'_I$ transitions contribute significantly to the spectral shape (Fig. 1). The powder pattern of the echo-detected EPR intensity $\boldsymbol{I}(H_0, \tau)$ for different pulse separation

times can be obtained by integration over all orientations of the molecule:

$$I(H_0, \tau) = \sum_{M_I, M_I'} \iint \sin\theta \, d\theta \, d\varphi \, P_{M_I, M_I'}(\theta, \varphi) e^{-\frac{2\tau}{T_2(\theta,\varphi)}} \times f(H_{res}(\theta, \varphi, M_I, M_I') - H_0, \Delta) \quad (8)$$

In this equation, the inhomogeneous line broadening due to unresolved hyperfine interactions with the surrounding protons is taken into account by a Gaussian line-shape function f with the width Δ.

The orientation-dependent relaxation rate $1/T_2$ describes the impact of the relaxation on the EPR line shape. In the following sections it is calculated for different relaxation-inducing mechanisms.

Relaxation mechanisms

To calculate the relaxation rates, we assume that the relaxation is caused by fast Larmor frequency fluctuations ($\Delta\omega\tau_c \ll 1$). Under this condition, the Redfield theory of relaxation[32] can be applied, and the orientation-dependent relaxation rates are given by:

$$\frac{1}{T_2(\theta, \varphi)} = \overline{\Delta\omega^2(\theta, \varphi)} J(0) + \frac{1}{2T_1} \quad (9)$$

where $J(0)$ is the spectral density at zero frequency, which we identify as the motional correlation time τ_c. We assume that the non-adiabatic term $1/2T_1$ can be neglected, since the longitudinal relaxation rates in all frequency bands are found to be much smaller than the transverse relaxation rates. In addition, we neglected spectral diffusion due to relaxation of the nitrogen nuclear spin. To calculate the amplitudes of the Larmor frequency fluctuations $\overline{\Delta\omega^2}$ we used the following Taylor series assuming small-angle excursions of the molecule:

$$\Delta\omega = \frac{\partial\omega_{M_I, M_I'}}{\partial\theta}\Delta\theta + \frac{\partial\omega_{M_I, M_I'}}{\partial\varphi}\Delta\varphi + \cdots \quad (10)$$

where the transition frequencies $\omega_{M_I, M_I'} = (E_{M_I} - E_{M_I'})/\hbar$, E_{M_I}, $E_{M_I'}$ are determined by Eqn (3).

Restricted motion around one molecular axis

If a molecule fluctuates with an angular amplitude α about an axis defined by the Euler angles Θ and Φ in the molecular frame (Fig. 2), the deviation of the Larmor frequency can be calculated by the following expression[23]:

$$\hbar\Delta\omega(\theta, \varphi) = \frac{\partial(E_{M_I} - E_{M_I'})}{\partial\theta}\Delta\theta + \frac{1}{\sin\theta}\frac{\partial(E_{M_I} - E_{M_I'})}{\partial\varphi}\Delta\varphi \quad (11)$$

where

$$\Delta\theta = \sin\Theta \sin(\Phi - \varphi)\alpha \quad (12a)$$

$$\Delta\varphi = (\cos\theta \sin(\Phi - \varphi) - \sin\theta \cos\Theta)\alpha \quad (12b)$$

By inserting Eqns (12a) and (12b) into Eqn (11), one obtains:

$$\overline{\Delta\omega^2(\theta, \varphi)} = \frac{\overline{\alpha^2}}{\hbar^2}\left(\frac{\partial(E_{M_I} - E_{M_I'})}{\partial\theta}\sin\Theta\sin(\Phi - \varphi) + \frac{1}{\sin\theta}\frac{\partial(E_{M_I} - E_{M_I'})}{\partial\varphi}(\cos\theta\sin(\Phi - \varphi) - \sin\theta)\right)^2 \quad (13)$$

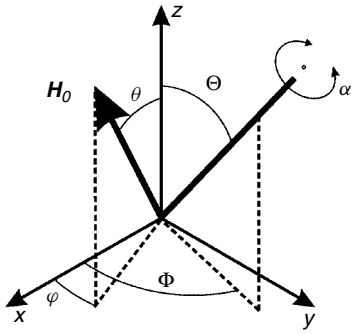

Figure 2. Relative orientation of the molecular axis system (x-, y- and z-axes) with respect to the external magnetic field vector $\boldsymbol{H}_0$ which is defined by the angles θ and φ. The angles Θ and Φ determine the orientation of an axis around which the molecule is fluctuating with an amplitude α.

Isotropic restricted motion

Isotropic motion can be described as a superposition of independent fluctuations of two polar coordinates $\Delta\theta$ and $\Delta\varphi$.

Calculating the angular gradients of the Larmor frequency, one obtains:[21]

$$\overline{\Delta\omega^2(\theta, \varphi)} = \frac{\overline{\alpha^2}}{\hbar^2}\left(\left(\frac{\partial(E_{M_I} - E_{M_I'})}{\partial\theta}\right)^2 + \frac{1}{\sin^2\theta}\left(\frac{\partial(E_{M_I} - E_{M_I'})}{\partial\varphi}\right)^2\right) \quad (14)$$

Dynamic *g*-strain

It is well known that the magnetic parameters of nitroxides are sensitive to interactions with the environment via polar groups or hydrogen bonds.[42,43] Thus, fluctuations of the local electric fields produced by surrounding solvent molecules modulate the **g**-matrix values (dynamic g-strain) and lead to anisotropic transverse relaxation.[22] To simulate the influence of the dynamic g-strain on the shape of the ED-EPR spectrum we assume that fluctuations of the g-values are caused by fluctuations of the electric field in the surrounding of the N–O fragment. To keep the theoretical treatment simple, only the dominating component of the electric field parallel to the axis of the N–O fragment was taken into account, which was assumed to affect only the principal values of the **g**-matrix, but not its orientation.

In theoretical[43] and experimental[44] studies on nitroxide molecules it was found that such E-field fluctuations mainly affect the canonical x-component of the **g**-matrix, i.e. g_{xx} is most sensitive to changes in the molecular environment. With these assumptions, the amplitude of the Larmor frequency fluctuations can be calculated with the following expression:

$$\overline{\Delta\omega^2(\theta, \varphi)} = \frac{\Delta g_{xx}^2}{\hbar^2}\beta^2 \sin^4\theta \cos^4\varphi |\boldsymbol{H}_0|^2 \quad (15)$$

where Δg_{xx} is the amplitude of the **g**-matrix fluctuations.

If several statistically independent relaxation processes affect the spin system, the echo decay can be calculated by a multiplication of the decays of each process. To calculate

the orientation-dependent relaxation times, we reformulated Eqn (9) to the following model-independent expression:

$$\frac{1}{T_2(\theta, \varphi)} = K(g_{ii}, A_{ii}, \theta, \varphi, H_0)\lambda \qquad (16)$$

where $K(g_{ii}, A_{ii}, \theta, \varphi, H_o)$ is a function of the g- and A-values, the nitroxide orientation and the external magnetic field. K is determined by the motional model. λ has different meanings for different relaxation mechanisms. It is equal to $\overline{\alpha^2}\tau_c$ for reorientational fluctuations of the molecule (Eqns 13 and 14) and to $\overline{g_{xx}^2}\tau_{cg}$ for modulations of the g_{xx}-component (Eqn 15), where τ_{cg} is the correlation time of the g-strain fluctuation.

Simulation of the echo-detected spectra

With the expressions derived above, the influence of molecular motion on the shape of the nitroxide ED-EPR spectrum was calculated. Figure 3 shows simulations for resonance frequencies in X-band (left column) and W-band (right column). In the five rows of Fig. 3 the impact of anisotropic relaxation induced by isotropic restricted motion (a), restricted molecular motion about the x-axis (b), y-axis (c), z-axis (d) and by dynamic g-strain (e) are shown. For each case, spectra with different pulse separation times τ were simulated. We chose simulations for these two frequency bands because they show characteristic features of the anisotropic relaxation at high and low resonance frequencies. To emphasize the changes in the spectral shape induced by anisotropic relaxation, we normalized all spectra to their maximum amplitude. From the simulations, it can be seen that relaxation induced by orientational fluctuations leads to smaller relaxation rates at the canonical positions than at the intermediate positions. As a result, the spectral shape changes with increasing pulse separation time, since the echo intensity at the fast relaxing positions vanishes faster than at the slowly relaxing positions.

Moreover, for motion around a canonical axis, the relaxation rate at the spectral position corresponding to the librational axis is smaller than the rate corresponding to the other two canonical positions. This allows discriminating between different types of molecular motion from a previously qualitative inspection of the W-band spectra where all three canonical values of the **g**-matrix are resolved. In general, as one can see from Fig. 3, W-band spectra are much more sensitive to the geometry of the motion than spectra obtained at X-band.

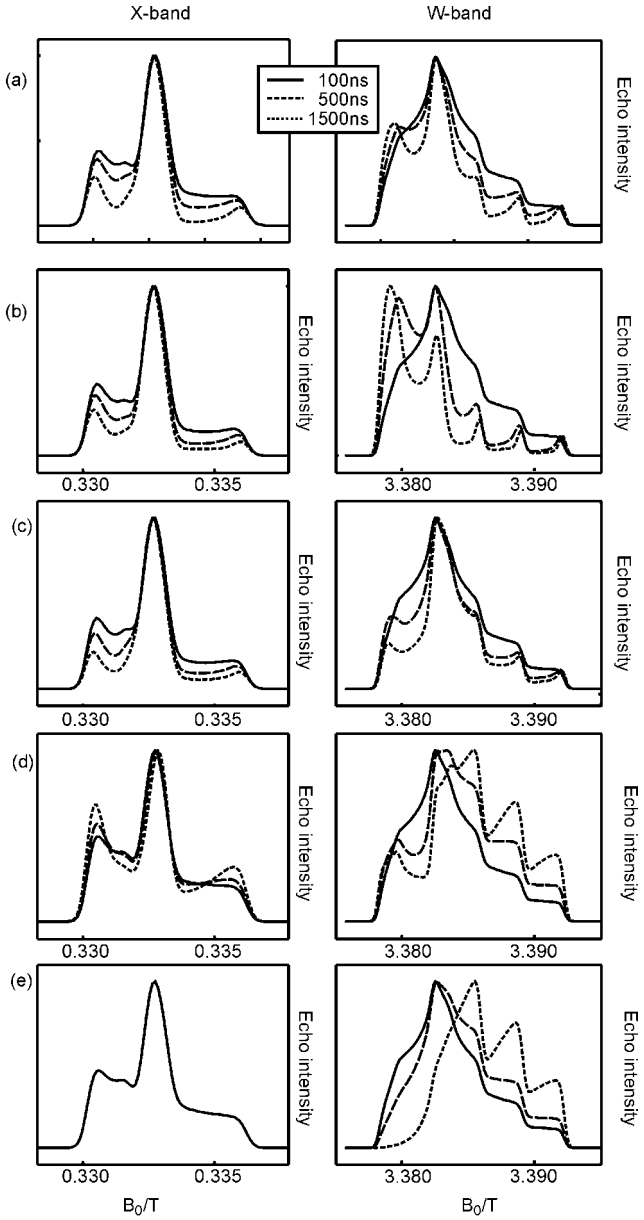

Figure 3. Simulations of the ED-EPR spectra of the nitroxide Fremy's salt calculated for X- (left column) and W-band (right column) resonance frequencies. In each picture, spectral simulations for different pulse separation times are shown, which are normalized to their maximum amplitude. In the spectral simulations, different relaxation-inducing mechanisms were included: (a) isotropic orientational excursions; (b) orientational excursions around the molecular x-axis; (c) orientational excursions around the molecular y-axis; (d) orientational excursion around the molecular z-axis; (e) dynamic g-strain.

RESULTS AND DISCUSSION

In the right column of Fig. 4, experimental ED-EPR spectra of Fremy's salt in glycerol glass ($T = 185$ K) at four different frequency bands (S-, X-, W- and G-bands) and at different pulse separation times are shown. The temperature of 185 K, which is close to the glass transition of glycerol, was chosen for experimental reasons. Below 185 K, the effect of the anisotropic relaxation is so small compared to the isotropic relaxation that it can hardly be observed at low magnetic fields.[21] At higher temperatures, however, the relaxation rates at high magnetic field are too large to enable evaluation of the relaxation anisotropy with adequate accuracy. The width of the nitroxide spectrum increases from ~5 mT at S-band to ~20 mT in G-band because of the magnetic field dependence of the electron Zeeman interaction. Upon increasing the resonance frequency, we found significantly increased relaxation rates when going from S- to G-band. In all frequency bands, changes of the line shape with increased pulse separation time were observed, which are induced by orientation-dependent relaxation. To demonstrate the

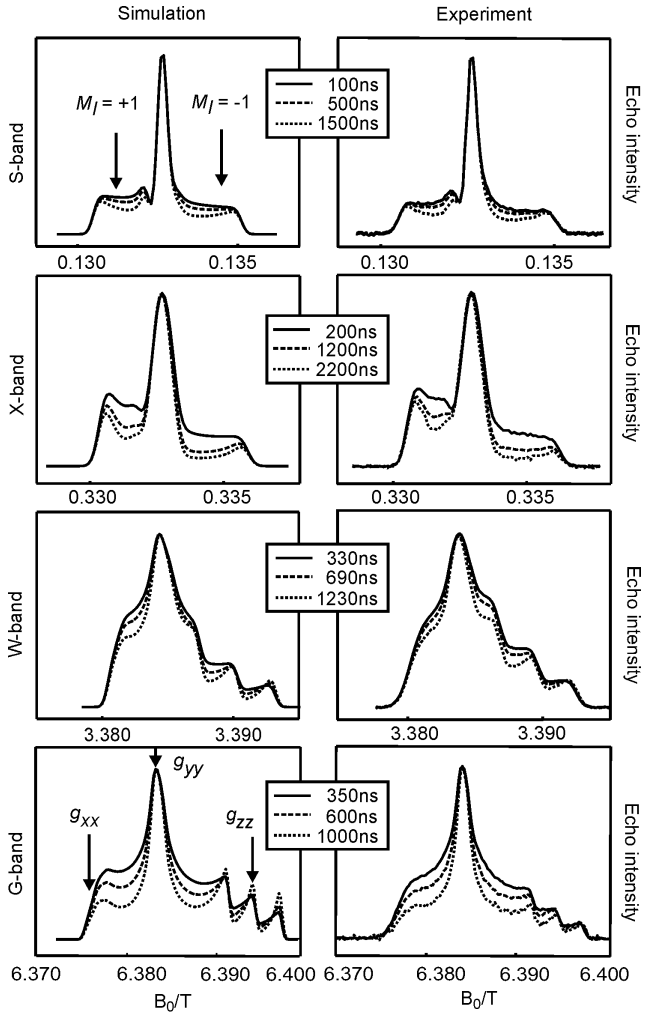

Figure 4. ED-EPR spectra of Fremy's salt at different pulse separation times at S-, X-, W- and G-bands; right column: experimental results in glycerol glass at $T = 185$ K; left column: simulations. In each box, spectra corresponding to different pulse separation times are shown, which were normalized to the maximum echo amplitude. The spectra were simulated using a model in which isotropic motion was superimposed by dynamic *g*-strain. The simulation parameters are given in Table 3.

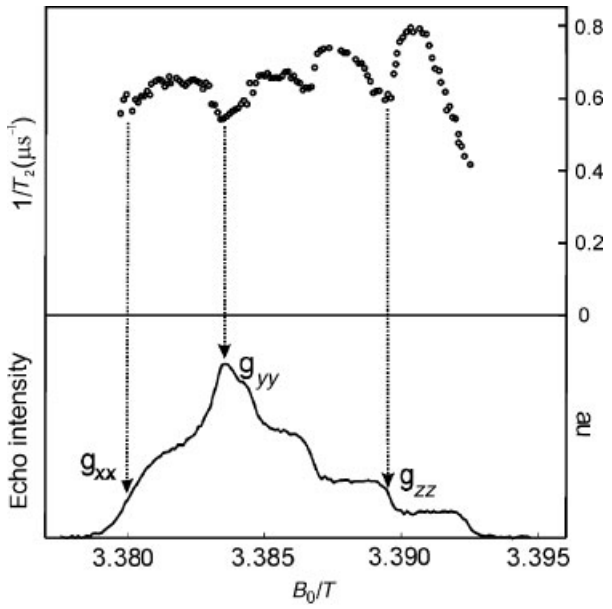

Figure 5. Transverse relaxation rates $1/T_2$ (upper part of the figure) of Fremy's salt in glycerol glass ($T = 185$ K) extracted from echo-decay functions at different positions in the W-band EPR spectrum (lower part of the figure $\tau = 100$ ns). The arrows indicate the spectral positions of the canonical *g*-values. The insert shows the two-pulse sequence applied to measure the echo decay.

strong dependence of the transverse relaxation rates on the resonance position, transverse relaxation rates of Fremy's salt measured at different field positions in the W-band EPR spectrum are shown in Fig. 5. The relaxation rates were obtained by fitting mono-exponential functions to the experimental echo decays. To exclude the isotropic relaxation from further considerations, we normalized the spectra in Fig. 4 to their maxima.

The following characteristic changes in the echo-detected spectra can be observed when changing the resonance frequency:

At S- and X-bands, where the spectral shape is mainly determined by the anisotropy of the axial hyperfine tensor, the relaxation rates at the parallel and perpendicular orientations of the **A**-tensor and of the central component of the spectrum are much smaller than at the intermediate positions. At X-band, the relaxation rate at the hyperfine component corresponding to $M_I = -1$ is larger than at the $M_I = +1$ component. At S-band, however, the same rates are observed at both components. This finding is due to the fact that at X-band, in contrast to S-band, the **g**-matrix anisotropy influences the relaxation. At X-band, at the $M_I = +1$ component, the hyperfine and **g**-matrix anisotropies partially compensate each other, while at $M_I = -1$ the **g**- and hyperfine anisotropies add, leading to an increase in $\Delta\omega$ and, thereby, to larger relaxation rates.

Upon approaching high-field EPR at W- and G-bands, pronounced changes can be observed concerning both the spectral shape and the anisotropy of the transverse relaxation rates. While at S- and X-bands the spectrum is dominated by the hyperfine anisotropy, at W- and G-bands the g_{xx}-, g_{yy}- and g_{zz}-matrix components are resolved. Therefore, the relaxation rates in W-band have five minima: one at the g_{xx}- and at the g_{yy}-components, respectively, and three at the g_{zz}-component, which is split by the hyperfine component A_{zz}. In G-band, we found a similar relaxation pattern. However, the g_{xx}-component showed bigger relaxation rates compared to the g_{yy}- and the g_{zz}-components, which was found to be nearly the same as the intermediate positions.

The observed relaxation pattern clearly indicates that the anisotropic relaxation is the result of molecular reorientational motion, which modulates both parts of the spin Hamiltonian – the electron Zeeman and the hyperfine interaction.

Before simulating the pulsed EPR spectra as a function of the pulse separation time, we had to check experimentally whether the assumption that the relaxation is induced by fast restricted motion of the nitroxide molecules is justified. This assumption was made to derive the theoretical

expressions Eqns (9) and (16). As described above, fast restricted motion should lead to mono-exponential echo decays and a quadratic dependence of the relaxation rates on the external magnetic field. Our experiments revealed mono-exponential decays within experimental accuracy at all spectral positions and for all frequency bands (data not shown). The field dependence, i.e. the dependence of the relaxation rates on $\Delta\omega$ can be checked by comparing the echo-decay rates of defined molecular orientations at two resonance frequencies. This can be done best by comparing relaxation rates obtained at two different high magnetic fields, where spectral shape is dominated by the anisotropy of the **g**-matrix, and $\Delta\omega$ depends quadratically on the external magnetic field.

Table 2 shows the transverse relaxation rates at the canonical orientations g_{yy} and at the intermediate position $1/2(g_{xx} + g_{yy})$ which were measured in W- and G-band EPR spectra. Going from W-band (95 GHz) to G-band (180 GHz) and, thereby increasing the resonance frequency by a factor of 1.89, all relaxation rates increase. To quantify the dependence of the anisotropic relaxation rates on the resonance frequency, we compared the differences of the relaxation rates at the canonical and the intermediate positions of the spectrum, thus excluding the impact of the isotropic relaxation processes. One can see from Table 2 that the difference between the relaxation rate at the g_{yy}-position and the relaxation rate between the g_{xx}- and the g_{yy}-positions change from $1.2 \pm 0.2 \times 10^{-5}$ s^{-1} (W-band) to $4.7 \pm 0.5 \times 10^{5}$ s^{-1} (G-band). At high magnetic fields, molecular fluctuations predominantly result in a modulation of the electron Zeeman interaction by reorientations of the anisotropic **g**-tensor. According to Eqn (1), the relaxation rates then depend quadratically on the external magnetic field. By increasing the resonance frequency from W- to G-band by a factor of $180/95 = 1.89$, the anisotropic relaxation rate increases by a factor of $4.7/1.2 = 3.9 \pm 0.4$, which is in perfect agreement with the factor of $(1.89)^2 = 3.6$, as predicted by the quadratic field dependence of the relaxation rate in Redfield theory.

Comparing the relaxation enhancement when going from S- to X-band EPR, these findings could be reproduced. The predicted trend was found when comparing X- and W-band results. However, a precise comparison of relaxation rates obtained at different positions in the X- and W-band spectra is difficult, since the dominating line-broadening mechanism, and therefore the orientation selection in the EPR spectra, is different. Nevertheless, a simultaneous simulation of X- and W-band data at different pulse separation times reveals equivalent information.

Table 2. Transverse relaxation rates of Fremy's salt in glycerol ($T = 185$ K) measured at the canonical position g_{yy} and at the intermediate position $1/2(g_{xx} + g_{yy})$ in W- and G-band EPR spectra

Spectral position	$1/T_2(10^5$ s$^{-1})$ (W-band)	$1/T_2(10^5$ s$^{-1})$ (G-band)
$1/2\,(g_{xx} + g_{yy})$	6.6 ± 0.1	14.5 ± 0.4
g_{yy}	5.4 ± 0.1	9.8 ± 0.1

On the basis of these findings, we conclude that the anisotropic relaxation is induced by fast restricted fluctuations of the molecule, which fulfil the necessary conditions of applicability of Redfield theory, i.e. $\Delta\omega\tau_c \ll 1$, which leads to $\tau_c \ll T_2 = 10^{-6}$ s. A lower limit of the correlation time can be derived from the observation that at all frequency bands, the longitudinal relaxation rate is smaller than the transverse relaxation rate by more than an order of magnitude. In the fast-motion limit, this leads to the relation $\omega_0\tau_c \gg 1$ with the electron resonance frequency ω_0. Inserting 3 GHz (S-band), the smallest applied Larmor frequency, we derive a lower limit for $\tau_c \gg 10^{-10}$ s. Putting together these facts, we conclude that the motional correlation time is between 10^{-7} and 10^{-10} s.

Comparing the simulations presented in Fig. 3 with the highly resolved W- and G-band spectra in Fig. 4, information about the geometry of the molecular motion can be extracted. In W-band and even more pronounced in G-band, the relaxation rate at the g_{xx}-position, $1/T_{2x}$, is larger than $1/T_{2y}$ and $1/T_{2z}$, the rates at the g_{yy}- and g_{zz}-positions respectively. Hence, molecular reorientations around the x- and z-axes can be ruled out as relaxation-determining process. Motion about the x- and z-axes would lead to $1/T_{2x} \ll 1/T_{2y}$, $1/T_{2z}$ and $1/T_{2z} \ll 1/T_{2x}$, $1/T_{2y}$ respectively, which is in contradiction with our experimental findings. Dynamic g-strain can be also excluded as main relaxation mechanism since the simulations cannot reproduce the observed relaxation pattern in the high-field spectra. In addition, dynamic g-strain does not lead to anisotropic relaxation in S- and X-bands. Nevertheless, at W- and G-bands, dynamic g-strain could be superimposed on the reorientation process and could contribute to the increased relaxation rates at g_{xx}.

For a quantitative characterization of the motional processes, the theoretical expressions derived above were fitted to the experimental spectra. In the fitting procedure, spectra obtained at different pulse separation times were simulated for all frequency bands simultaneously with a single parameter set. We found that isotropic motion alone cannot explain the experimental spectra. Although it leads to strong differences in the relaxation rates between the intermediate and the canonical orientations, as was observed in the experiment, the simulations with this isotropic model cannot reproduce the enhanced relaxation at the x-component of the W- and G-band spectra. This feature can only be explained by an effect that modulates the Larmor frequency at the g_{xx}-component of the **g**-matrix more strongly than at the other canonical orientations. Such modulations can either be the result of dynamic g-strain, which mainly affects the g_{xx}-value, or of motion around the y-axis, which would also induce a larger relaxation rate at the g_{xx}-position.

To reproduce the observed relaxation behaviour, we performed fits to two motional models: isotropic orientational motion superimposed by dynamic g-strain and orientational excursions about all three canonical orientations with larger amplitude about the molecular y-axis.

Simulations with both models yield good agreement with the experimental ED-EPR spectra. The best agreement between simulations and experiments, however, was found for isotropic motion overlapped by dynamic g-strain. In

Table 3. Simulation parameters for the model of isotropic motion with dynamic *g*-strain assessed by comparing least-square fits of the simulated ED EPR spectra to the experimental data

$A_{xx}/(\hbar\gamma_e)$	0.50 ± 0.02 mT
$A_{yy}/(\hbar\gamma_e)$	0.43 ± 0.02 mT
$A_{zz}/(\hbar\gamma_e)$	2.80 ± 0.01 mT
g_{xx}	2.0080 ± 0.0001
g_{yy}	2.0058 ± 0.0001
g_{zz}	2.0026 ± 0.0001
Δ	0.31 ± 0.01 mT
$\overline{\alpha^2}\tau_c$	$(8 \pm 1) \times 10^{-13}$ rad^2 s
$\overline{g_{xx}^2}\tau_{cg}$	$(1.3 \pm 0.5) \times 10^{-13}$ s

the left column of Fig. 4 simulations of S-, X-, W- and G-band ED-EPR spectra are shown, which were calculated for the same pulse separation times as the experimental spectra. The simulations were performed with the best set of fit parameters listed in Table 3. With this model we were able to reproduce all characteristic features induced by anisotropic relaxation in the ED-EPR spectra. Only in G-band ED-EPR a discrepancy remains between the simulated and the measured spectra. The simulations show a minimum of the relaxation rates between g_{xx} and g_{yy}, and the g_{zz}-component relaxes slower than g_{yy}, which is not the case in the experiment.

Although the fits including the *g*-strain model yield better results, they do not provide a decisive criterion as to which of two motional processes actually dominates the anisotropic relaxation.

Motion around the molecular *y*-axis may be explained by the hydrogen-bond network which fixes the nitroxide in the solvent cage. In polar solvents, Fremy's salt forms 14 hydrogen bonds with the solvent molecules, six to each of the SO_3 fragments (Scheme 1) and two to the N–O fragment. Such a hydrogen-bond network leads to a strong binding axis in the *y*-direction, which restricts excursions about the *x*- and *z*-axes.

Dynamic *g*-strain can be induced by fluctuations of the local electric fields or of hydrogen bonds. A static distribution of the local environment is already apparent in the continuous-wave high-field EPR spectrum, where a pronounced broadening of the g_{xx}-component can be observed (data not shown). Fluctuations between these conformational substates induce Larmor frequency fluctuations, which mainly effect the transverse relaxation on g_{xx}.

In order to decide which of these two mechanisms induces the observed anisotropic relaxation, we compared our results with independent inversion–recovery and ELDOR measurements on nitroxides in glasses.[12,45] In these studies it was found that, similar to the transverse relaxation rate, the longitudinal relaxation rate $1/T_1$ shows a pronounced dependence on the spectral position. The smallest longitudinal relaxation rates were observed at the spectral positions where mainly the *x*- and *y*-orientations are selected, while the positions with selected *z*-orientation relax more slowly. These findings were explained by a modulation of the canonical **g**-matrix values. Since both the transverse and the longitudinal relaxation rates are a function of the amplitude and the correlation time of the Larmor frequency fluctuations, dynamic *g*-strain should also manifest itself in the transverse relaxation rate.

By means of the general expression $1/T_2 \geq 1/T_1$, the impact of the dynamic *g*-strain on the transverse relaxation can be estimated. Measurements of the difference between the longitudinal relaxation rates of Fremy's salt ($T = 190$ K) at the *z*- and *x*-positions[46] revealed $1/T_{1x} - 1/T_{1z} = 0.5 \times 10^4$ s^{-1}. Since $1/T_{2x} - 1/T_{2z} \geq 1/T_{1x} - 1/T_{1z} = 0.5 \times 10^4$ s^{-1}, this value is the lower limit for the transverse relaxation induced by dynamic *g*-strain in X-band. Upon increasing the external magnetic field, dynamic *g*-strain leads to increased relaxation rates due to the quadratic field dependence of $1/T_2$. In our measurements, the external magnetic field was increased by a factor of 20 from X- to G-band, which leads to 400 times larger anisotropic relaxation rates. This estimate is in accordance with the observed anisotropic relaxation rate of $1/T_{2x} - 1/T_{2z} = 0.5 \times 10^6$ s^{-1}. Therefore, we suggest that in the Fremy's salt in glycerol at 185 K, the transverse relaxation is determined by fast isotropic fluctuations of the spin probes in the solvent cage, which are overlapped by dynamic *g*-strain effects. The remaining differences between the spectral simulations and the experimental data, especially in the region between g_{xx} and g_{yy}, may be due to an oversimplified model of the *g*-strain. In the described model, the fluctuating electric fields manifest themselves only in fluctuations of the principal **g**-matrix values, whereas such fluctuations can also change the orientation of the **g**-matrix axes system relative to the nitroxide skeleton. In addition, the fluctuating electric fields actually may be more complicated than the simple model of an electric field parallel to the N–O axis.

The presented data show how pulsed ED-EPR at different resonance frequencies can be used to investigate molecular motion in disordered media. Especially, the high spectral resolution of high-field/high-frequency EPR dramatically increases the information content that can be extracted from the ED-EPR spectra. In addition, measurements at different high magnetic fields allow the determination of the timescale of motion. This is indispensable information for a proper interpretation of the anisotropic relaxation. Benefiting from these advantages, we were able to identify the origin of the anisotropic relaxation.

Our study shows that near the glass transition temperature the orientation-dependent transverse relaxation of Fremy's salt in frozen glycerol can be described by analytical expressions in the framework of Redfield's relaxation theory. Above the glass transition temperature, however, the relaxation rates are more and more dominated by slow motion of the solvent cage.[13,26] Such processes can no longer be treated in the framework of Redfield theory but need a more general treatment as was developed, for example, by Freed and co-workers.[38,47,48]

CONCLUSION

Pulsed EPR measurements were performed at microwave frequencies of 3, 9.5, 95 and 180 GHz to investigate the origin

of the anisotropic transverse relaxation rates of Fremy's salt near the glass transition temperature of glycerol. By increasing the magnetic field and thereby the resonance frequency, the overall relaxation rates and their anisotropy increase. At all frequency bands, anisotropic relaxation was observed with smaller relaxation rates at the canonical spectral positions of the hyperfine and **g**-matrices as compared to the intermediate positions. In G-band ED-EPR spectra, we found increased relaxation rates at the g_{xx}-component compared to the other two canonical positions.

From these findings, we assign the anisotropy of the transverse relaxation rates to molecular reorientations simultaneously modulating the hyperfine and **g**-matrices. Measurements at two different high Larmor frequencies showed a quadratic dependence of the anisotropic relaxation rates on the external magnetic field. This allows us to estimate the timescale of the motional process $10^{-10}\ \mathrm{s} < \tau_c < 10^{-7}\ \mathrm{s}$, i.e. at $T = 180\ \mathrm{K}$, the motion occurs in the fast-motion Redfield regime.

On the basis of Redfield's relaxation theory, we developed motional models that describe different kinds of molecular reorientations and compared them with the experimentally obtained multi-frequency relaxation data.

Fits of the spectral simulations to the experimental results show good agreement for two different relaxation models: (i) isotropic orientational motion superimposed by dynamic *g*-strain and (ii) orientational excursions about all three canonical orientations with a larger excursion about the molecular *y*-axis of the nitroxide molecule.

A quantitative comparison of the orientation dependence of the transverse relaxation rates with independent measurements of the longitudinal relaxation rates by X-band EPR show that the increased relaxation rate at the g_{xx}-position can be explained by dynamic *g*-strain. To separate the contributions of dynamic *g*-strain and motion around the molecular *y*-axis, multi-frequency experiments on nitroxides with different shapes are necessary. By restricting the motional freedom of the nitroxide in its solvent pocket in a geometrically controlled way, it should be possible to disentangle the two mechanisms.

The presented results demonstrate the potential of pulsed, multi-frequency EPR measurements to study both timescales and motional modes in supercooled media around the glass transition temperature. Measurements on site-specifically labelled protein samples are in progress to use the described method to gain detailed information about the complicated motional modes in protein glasses. Such information is important to understand the biological processes in proteins at the molecular level.

Acknowledgements

We are grateful to Dr Anton Savitsky for help with the W-band experiments and Drs Alexander G. Maryasov, Michael Fuhs and Alexander B. Doktorov for helpful discussions on the theory of spin relaxation. This work was supported by the INTAS (YSF 2002-410/F1b), the Deutsche Forschungsgemeinschaft (SPP 1051, SFB 498) and the Russian Foundation for Basic Research (grant 04-03-32211), which are gratefully acknowledged.

REFERENCES

1. Angell CA, Ngai KL, McKenna GB, McMillan PF, Martin SW. *J. Appl. Phys.* 2000; **88**(6): 3113.
2. Debendetti PG, Stillinger FH. *Nature* 2001; **410**: 259.
3. Onuchic JN, Luthey-Schulten Z, Wolynes PG. *Annu. Rev. Phys. Chem.* 1997; **48**: 545.
4. Parak F, Frolov EN, Kononenko AA, Mössbauer RL, Goldanskii VI, Rubin AB. *FEBS Lett.* 1980; **117**(1–2): 368.
5. Frauenfelder H, McMahon BH, Fenimore PW. *Proc. Natl. Acad. Sci.* 2003; **100**(15): 8615.
6. Dzuba SA, Tsvetkov YD. *Khim. Fiz.* 1982; **9**(1): 1197.
7. Dzuba SA, Maryasov AG. *J. Magn. Reson.* 1984; **58**: 95.
8. Millhauser GL, Freed JH. *J. Chem. Phys.* 1984; **81**(1): 37.
9. Lebedev Y. High-frequency continuous-wave electron spin resonance. In *Modern Pulsed and Continuous Wave Electron Spin Resonance*, Kevan L, Bowman MK (eds). Wiley: New York, 1990; 365.
10. Dzuba SA. *Pure Appl. Chem.* 1992; **64**(6): 825.
11. Rohrer M, Gast P, Möbius K, Prisner TF. *Chem. Phys. Lett.* 1996; **259**(5–6): 523.
12. Saalmueller JW, Long HW, Maresch GG, Spiess HW. *J. Magn. Reson., Ser. A* 1997; **117**(2): 193.
13. Saxena S, Freed JH. *J. Phys. Chem. Ser. A* 1997; **101**(43): 7998.
14. Zecevic A, Eaton GR, Eaton SS, Lindgren M. *Mol. Phys.* 1998; **95**(6): 1255.
15. Barbon A, Brustolon M, Maniero AL, Romanelli M, Brunel L-C. *Phys. Chem. Chem. Phys.* 1999; **1**(17): 4015.
16. Schnegg A, Fuhs M, Rohrer M, Lubitz W, Prisner TF, Möbius K. *J. Phys. Chem. B* 2002; **106**: 9454.
17. Leoporini D, Schädler V, Wiesener U, Spiess HW, Jeschke G. *J. Chem. Phys.* 2003; **119**(22): 11 829.
18. Fremy E. *Ann. Chim. Phys.* 1845; **15**: 408.
19. Dzuba SA, Tsvetkov YA. *Appl. Mag. Reson.* 1990; **1**: 179.
20. Milov AD, Salikhov KM, Tsvetkov YD. *Sov. Phys. Solid State Phys.* 1973; **15**(4): 1187.
21. Kirilina EP, Dzuba SA, Maryasov AG, Tsvetkov YD. *Appl. Magn. Reson.* 2001; **21**(2): 203.
22. Poluektov OG, Doubinski AA. *Chem. Phys. Lett.* 1998; **288**(5–6): 841.
23. Dzuba SA. *Spectrochim. Acta A* 2000; **56**: 227.
24. Maresch GG, Weber M, Dubinskii AA, Spiess HW. *Chem. Phys. Lett.* 1992; **193**(1–3): 134.
25. Vorobiev AK, Gurman VS, Klimenko TA. *Phys. Chem. Chem. Phys.* 2000; **2**(2): 379.
26. Bonora M, Pornsuwan S, Saxena S. *J. Phys. Chem.* 2003; **108**: 4196.
27. Peng JW, Wagner G. Investigation of protein motions via relaxation measurements. In *Nuclear Magnetic Resonance, Part C*, James T, Oppenheimer N, Abelson J, Simon M (eds). Elsevier: Amsterdam, 1994; 563.
28. Prisner TF, Rohrer M, Möbius K. *Appl. Magn. Reson.* 1994; **7**: 167.
29. Kutter C, Moll HP, Van Tol J, Zuckermann H, Wyder P. *Infr. Phys. Tech.* 1995; **36**(1): 245.
30. Rohrer M, Brüggmann O, Kinzer B. *Appl. Magn. Reson.* 2001; **21**: 257.
31. Blok H, Disselhorst JAJM, Orlinskii SB, Schmidt J. *J. Magn. Res.* 2003; **166**(1): 92.
32. Redfield AG. *Adv. Mag. Res.* 1965; **1**: 1.
33. Schwartz LJ, Stillman AE, Freed JH. *J. Chem. Phys.* 1982; **77**(11): 5410.
34. Zhidomirov GM, Salhikov KM. *Sov. Phys. JETP* 1969; **29**(6): 1037.
35. Klauder JR, Anderson PW. *Phys. Rev.* 1962; **125**: 912.
36. Hu P, Hartmann SR. *Phys. Rev. B* 1974; **9**: 1.
37. Earle KA, Budil DE, Freed JH. *J. Phys. Chem.* 1993; **97**(50): 13 289.
38. Polimeno A, Freed JH. *J. Phys. Chem.* 1995; **99**: 109 995.
39. Schweiger A, Jeschke G. *Principles of Pulse Electron Paramagnetic Resonance*. University Press: Oxford, 2001.
40. Weber A. Phd. thesis, Johann Wolfgang Goethe Universität, Frankfurt, 2002.
41. Savitsky A, Kühn M, Duché D, Möbius K, Steinhoff H-J. *J. Phys. Chem.* 2004; **108**(27): 9541.

42. Berliner LJ. Spin labelling theory and applications. *Molecular Biology*, Horecker B, Kaplan NO, Marmur J, Scheraga HA (eds). Academic Press: New York, San Francisco, London, 1976.
43. Plato M, Steinhoff H-J, Wegener C, Törring JT, Savitsky A, Möbius K. *Mol. Phys.* 2002; **100**(23): 3711.
44. Gullá AF, Budil DE. *J. Phys. Chem. B* 2001; **105**(33): 8056.
45. Du JL, More KM, Eaton SS, Eaton GR. *Isr. J. Chem.* 1992; **32**(2–3): 351.
46. Dzuba SA, Kirilina EP, Salnikov ES, Eaton S, Kulik LV. *J. Chem. Phys.* 2005; **122**: 94 702.
47. Earle KA, Moscicki JK, Polimeno A, Freed JH. *J. Chem. Phys.* 1997; **106**(24): 9996.
48. Barnes JP, Liang Z, Mchaourab HS, Freed JH, Hubbell WL. *Biophys. J.* 1999; **76**(6): 3298.